Dalton Transactions

PAPER

CrossMark
click for updates

Cite this: DOI: 10.1039/c5dt00368g

A novel inorganic–organic nanohybrid material $H_4SiW_{12}O_{40}$/pyridino-MCM-41 as efficient catalyst for the preparation of 1-amidoalkyl-2-naphthols under solvent-free conditions

R. Tayebee,*[a] M. M. Amini,[b] M. Akbari[a] and A. Aliakbari[b]

A new inorganic–organic nanohybrid material $H_4SiW_{12}O_{40}$/pyridino-MCM-41 was prepared and performed as an efficient, eco-friendly, and highly recyclable catalyst for the one-pot multi-component synthesis of different substituted 1-amidoalkyl-2-naphthols under solvent-free conditions. The nanohybrid catalyst was prepared through electrostatic anchoring of Keggin heteropolyacid $H_4SiW_{12}O_{40}$ on the surface of MCM-41 nanoparticles modified by N-[3-(triethoxysilyl)propyl]isonicotinamide. The prepared material was characterized by XRD, SEM, EDX, UV-Vis, DTA-TGA, DLS, and FT-IR spectroscopy. Findings confirmed that the heteropolyacid is well dispersed on the surface of the solid support and its structure is preserved after immobilization on the TPI modified MCM-41 nanoparticles. The recovered catalyst was easily recycled for at least seven runs without considerable loss of catalytic activity.

1. Introduction

Instability of homogeneous catalysts in reaction media and difficulty in recovery are the main disadvantages which prevent their practical applications in both synthetic chemistry and industrial processes. Therefore, preparing hybrid catalysts by linking homogeneous catalysts with organic linkers can provide materials which are easier to handle, and may exhibit improved selectivity and activities.[1] Inorganic–organic hybrid materials can be classified into two classes: (i) compounds in which weak interactions such as van der Waals forces, hydrogen bonds, or electrostatic interactions are created between organic and inorganic components, and (ii) inorganic–organic hybrid materials where both organic and inorganic components are bonded through strong covalent bonds.[2]

Since pure heteropolyacids generally show low catalytic activity owing to their small surface area, the catalytic function of Keggin $H_4SiW_{12}O_{40}$ (HPA) would be improved at the atomic and molecular level by anchoring to different porous materials with high surface area, such as MCM-41, which shows high thermal stability, large surface area, and good adsorption capacity for organic molecules.[3–7] MCM-41 is able to carry

high dosages of a variety of drugs in its mesopores, called drug delivery vehicles.[8–10] Furthermore, mesoporous MCM-41 contains a large number of free silanol groups on its surface which generate high specific surface areas and porosities; therefore, the surface silanol groups can be modified by reaction with suitable organic modifiers and new inorganic–organic hybrid mesoporous materials can thus be prepared.[11,12]

1-Amidoalkyl-2-naphthols are raw materials for many important biological purposes such as HIV protease inhibitors,[13,14] antibiotics,[15] antitumors,[16] antipsychotics,[17] and antihypertensives.[18] Therefore, synthesis of these significant compounds via catalytic green and efficient protocols is a prominent subject of interest. Although there are a number of reports on the three component condensation reaction of 2-naphthol, aldehydes and amides in the presence of different catalysts for the synthesis of 1-amidoalkyl-2-naphthols, the majority of these methods suffer from several limitations such as corrosive and expensive reagents, strongly acidic conditions, and harsh reaction conditions.[19,20]

In order to obtain an efficient heterogeneous catalyst, HPA was supported on TPI-MCM-41 to provide a highly dispersed hybrid material. The goal of this work was to characterize the new nanohybrid material and evaluate the catalytic activity of this heterogeneous catalyst in reference to the bulk heteropolyacid. Therefore, the prepared inorganic–organic nanohybrid material $H_4SiW_{12}O_{40}$/pyridino-MCM-41 would be a suitable candidate of choice for the efficient preparation of 1-amidoalkyl-2-naphthols under environmental benign conditions and principles of safe chemistry (Scheme 1).

[a]Department of Chemistry, School of Sciences, Hakim Sabzevari University, Sabzevar 96179-76487, Iran. E-mail: Rtayebee@hsu.ac.ir; Fax: +98-51-44410300; Tel: +98-51-44410310
[b]Department of Chemistry, Shahid Beheshti University, G.C., Tehran 1983963113, Iran
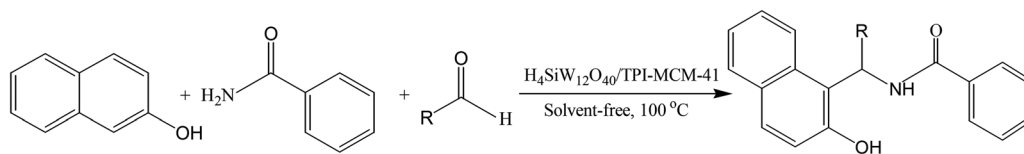
Scheme 1 General formulation for the preparation of different 1-amidoalkyl-2-naphthols.

2. Experimental

2.1. Materials and methods

Reagents and solvents were purchased from Merck or Fluka and used as received. The solid samples were identified by X-ray powder diffraction (XRD) using a STOE diffractometer with Cu-Kα radiation (λ = 0.15418 nm) at 40 kV and 40 mA. The diffraction patterns were recorded in the Bragg angle (2θ) range from 1° to 10° for small angle XRD and from 10° to 80° for wide-angle XRD, with a position sensitive detector using a step size of 0.06°. Infrared spectra were recorded (KBr pellets) on a 8700 Shimadzu Fourier Transform spectrophotometer applying the KBr technique in the range of 400 to 4000 cm^{-1}. The pellets for FT-IR analysis were made of ~3 mg of the nano-hybrid catalyst combined with approximately 250 mg of KBr. Thermogravimetry and differential thermal analysis (TGA-DTA) were carried out on a Bahr STA-503 instrument in air at a heating rate of 10 °C min^{-1}. Ultraviolet–visible spectra were recorded on a UV-Vis Array Spectrophotometer (Photonix Ar 2015, Iran) in the range of 200–800 nm. A Philips XL-30 ESEM scanning electron microscope (acceleration voltage 26 kV) equipped with an Oxford Energy Dispersive X-ray (EDX) spectrometer was used to observe morphology and perform microanalysis. The tungsten content in the nanohybrid catalyst was determined using inductively coupled plasma optical emission spectroscopy (ICP-OES) conducted on a Varian Vista-Pro model ICP-OES spectrometer. To determine the tungsten content, the wavelength of 239.708 nm was observed by ICP-OES analysis. Melting points were recorded on a Bamstead electrothermal type 9200 melting point apparatus. Hydrodynamic particle size analysis of HPA/TPI-MCM-41 in an ethanol suspension was determined by measuring the dynamic light scattering by a Zeta Sizer-HT (Brookhaven). Thin layer chromatography (TLC) was performed on Merck silica gel 60 F254 plates using ethyl acetate and hexane (1 : 4) as eluting agents. TLC plates were visualized by exposure to UV light. ^{1}H and ^{13}C NMR spectra were recorded on a Bruker AVANCE 100 MHz instrument using TMS as internal reference. All products were identified by comparison of their spectral and physical data with those previously reported.[21,22] Keggin heteropolyacid $H_4SiW_{12}O_{40}$ catalyst (HPA) was prepared according to the previously reported methods.[23]

2.2. Synthesis of MCM-41 mesoporous silica

MCM-41 mesoporous silica was synthesized by the sol–gel method according to the literature with slight modifications.[24] This material was crystallized from a gel with the molar com-

position SiO_2 : 0.2 hexadecyltrimethylammonium bromide (CTAB) : 120 H_2O. For this purpose, 34.91 g sodium silicate solution (7% Na_2O, 27% SiO_2) was diluted with 100 ml H_2O and was added slowly to a rapidly stirred solution of 11.85 g CTAB in 220 ml H_2O. A precipitate formed immediately which was stirred at ambient temperature for 30 min. Dilute sulfuric acid (2 M) was then added dropwise to adjust the pH of the gel to 10. After being stirred for 3 h and readjusting the pH, the synthesized gel was transferred to a Teflon-lined autoclave and heated to 150 °C for 36 h. The solid particles produced were collected by filtration, dried overnight at room temperature, and calcined in air at 540 °C for 6 h to remove the template.

### 2.3. Preparation of pyridine functionalizing agent

N-[3-(Triethoxysilyl)propyl]isonicotinamide (TPI) was synthesized according to the previously reported procedure and characterized by ^{1}H NMR.[25] Briefly, 4-pyridinecarboxylic acid (2.0 g, 16 mmol) was suspended in dry CH_2Cl_2 (100 ml) under nitrogen atmosphere. To this solution, oxalyl chloride (4.1 ml, 48 mmol) was slowly added and the mixture was stirred for 12 h. The CH_2Cl_2 was removed under reduced pressure and the residue was suspended again in dry CH_2Cl_2 (100 ml). After addition of triethylamine (6.7 ml, 48 mmol) to the reaction mixture, 3-aminopropyltriethoxysilane (3.8 ml, 48 mmol) was slowly added. The reaction mixture was stirred at room temperature for 4 h and then the mixture was suspended in water to remove impurities. The organic phase separated and the solvent was removed under reduced pressure to obtain a brownish viscous oil. The synthesis of TPI was confirmed by ^{1}H NMR (CDCl$_3$, ppm): 0.61 (t, 2H), 1.11 (t, 9H) 1.65 (m, 2H), 3.36 (m, 2H), 3.72 (q, 6H), 7.24 (d, 2H), 7.57 (s, 1H), 8.60 (d, 2H).

2.4. Synthesis of pyridine-functionalized MCM-41 (TPI-MCM-41)

The general sol–gel procedure for functionalization of nanoporous silica was used to functionalize Si-MCM-41.[26] In a typical reaction, 1.0 g of MCM-41 was suspended in 80 ml toluene and the mixture was stirred for 1 h; then, 2.5 ml of TPI was added and the mixture was refluxed for 48 h. The white-brown solid was removed from the solvent by filtration, washed with toluene and acetone and then dried at room temperature. FT-IR and TGA-DTA analyses showed TPI anchored onto the mesoporous support.

2.5. Immobilization of silicotungstic acid $H_4SiW_{12}O_{40}$ on TPI-MCM-41 (HPA/TPI-MCM-41)

For systematic access to the immobilized catalyst HPA/TPI-MCM-41, a modular system combining functionalized TPI
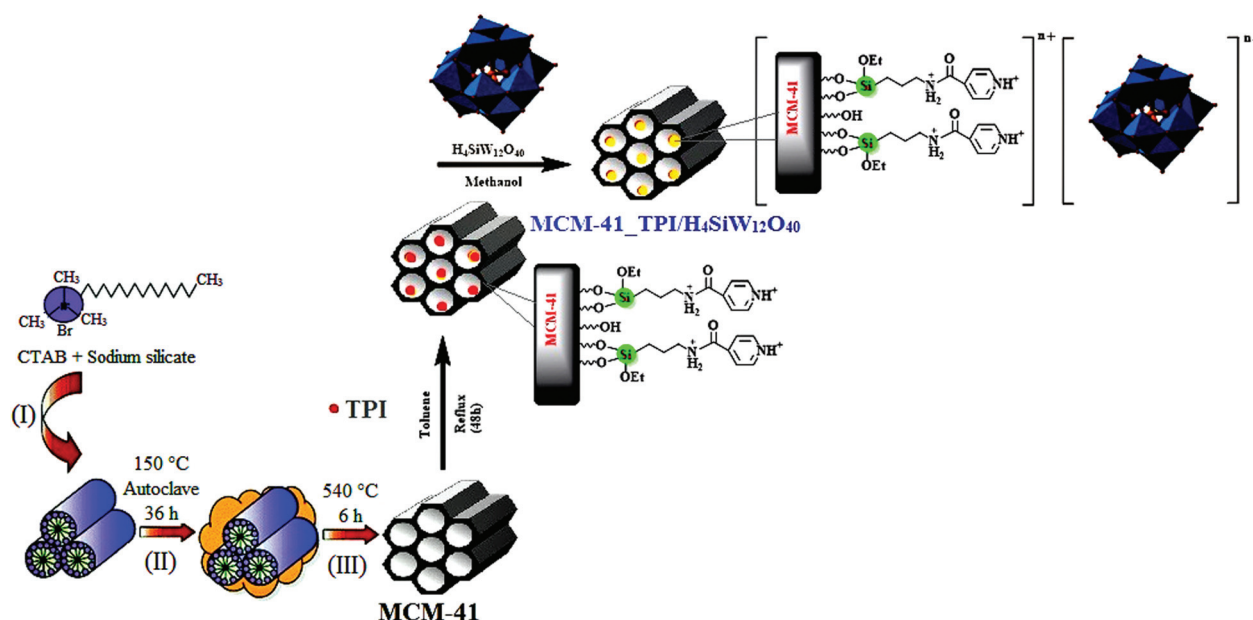
Scheme 2 A schematic diagram for the pyridine functionalization of MCM-41 mesoporous silica and immobilization of HPA.

was developed to immobilize $H_4SiW_{12}O_{40}$ on MCM-41 (Scheme 2). For the immobilization of the heteropolyacid on the functionalized MCM-41, 50 ml of methanol containing 0.7 g of $H_4SiW_{12}O_{40}$ was added to freshly prepared TPI-MCM-41 (1.0 g) and the mixture was refluxed for 4 h. Then, the heterogeneous catalyst was filtered off and washed with methanol several times and thereafter was dried at room temperature. XRD and FT-IR analysis of the prepared inorganic–organic nanohybrid catalyst confirmed anchoring of HPA onto the pyridine-functionalized silica. UV-Vis analysis showed about 0.09 mmol g^{-1} of HPA is loaded on TPI-MCM-41. The amount of 0.09 mmol g^{-1} was equivalent to coordination of HPA to about 8% of the total amount of TPI covalently attached to the MCM-41 surface, as calculated by TGA-DTA analysis. A schematic representation for the preparation of the HPA/TPI-MCM-41 nanocatalyst is shown in Scheme 2. The scheme shows grafting of TPI onto MCM-41 *via* condensation of hydroxyl and ethoxy groups of the support and linker, respectively; then, the HPA was anchored to TPI-MCM-41 *via* electrostatic interaction in the second step.

2.6. General procedure for the preparation of substituted 1-amidoalkyl-2-naphthols

In a typical reaction, a mixture of β-naphthol (1.0 mmol), aldehyde (1.0 mmol), benzamide (1.2 mmol), and HPA/TPI-MCM-41 (15 mg) in a small test tube equipped with a condenser was conventionally heated to 100 °C for the required time. After completion of the reaction monitored by TLC, the mixture was cooled to 25 °C, boiling ethanol was added and the mixture was stirred for 5 min. The catalyst was filtered off; then, the solution was cooled to room temperature and the resulting solid was filtered and re-crystallized from 15%

aqueous ethanol. Yields refer to the isolated yields in all catalytic tests. This general procedure was used for all catalytic tests, but with the mentioned amount of the used catalyst.

2.7. Spectral data for some selected 1-amidoalkyl-2-naphthols

2.7.1. *N*-[(2-Hydroxynaphthalen-1-yl)phenylmethyl]benzamide. White solid, ^{1}H NMR (DMSO-d$_6$) δ = 10.3 (br, s, 1H), 8.16–8.12 (m, 6H), 7.90–7.86 (m, 5H), 7.41 (br, s, 1H), 7.20–7.15 (m, 5H), 6.06 (s, 1H); ^{13}C NMR (DMSO-d$_6$) δ = 169, 153, 148, 145, 135, 133, 133, 132, 131, 130, 130, 128, 128, 128, 127, 124, 122, 121, 119, 118, 50.

2.7.2. *N*-(1-(2-Hydroxynaphthalen-1-yl)-3-phenylallyl)benzamide. White solid, ^{1}H NMR (DMSO-d$_6$): δ = 7.1 (d, 1H), 7.15 (d, 1H), 7.20 (m, 4H), 7.42 (m, 3H), 7.77 (m, 3H), 8.10 (d, 1H), 9.03 (d, 1H), 10.45 (s, 1H). ^{13}C NMR (DMSO-d$_6$): δ = 165, 158, 142, 137, 136, 133, 132, 131, 128, 127, 123, 48.

2.7.3. *N*-[4-Nitrophenyl-(2-hydroxynaphthalen-1-yl)methyl]benzamide. White solid, FT-IR (neat) = 3420, 3062, 1627, 1572, 1534, 1489, 1347, 1271, 1026, 942, 822, 750 cm^{-1}. ^{1}H NMR (DMSO-d$_6$): δ = 7.27 (m, 8H), 7.46 (t, 3H), 7.57 (d, 1H), 7.83 (m, 4H), 8.08 (d, 1H), 9.03 (d, 1H), 10.37 (br, s, 1H). ^{13}C NMR (DMSO-d$_6$): δ = 167, 154, 151, 146, 134, 133, 132, 130, 129, 128, 127, 124, 123, 119, 118, 49.

2.7.4. *N*-[4-Tolyl-(2-hydroxynaphthalen-1-yl)methyl]benzamide. Light yellow solid, ^{1}H NMR (DMSO-d$_6$, TMS) δ = 9.92 (br, s, 1H), 8.03–7.97 (m, 6H), 7.63 (br, s, 1H), 7.24–7.14 (m, 9H), 6.08 (s, 1H), 1.90 (s, 3H); ^{13}C NMR (DMSO-d$_6$) δ = 168, 153, 143, 140, 135, 133, 129, 129, 128, 126, 125, 123, 123, 120, 118, 48, 20.

2.7.5. *N*-(1-(2-Hydroxynaphthalen-1-yl)-3-phenylpropyl)-benzamide. White solid, ^{1}H NMR (DMSOd$_6$): δ = 2.03

(m, 2H), 2.75 (t, 2H), 5.98 (d, 1H), 7.12–7.24 (m, 6H), 7.41–7.47 (m, 4H), 7.68–7.83 (m, 4H), 8.02 (d, 1H), 8.68 (d, 1H), 10.17 (s, 1H). ^{13}C NMR (DMSO-d$_6$): δ = 165, 153, 142, 134, 132, 131, 128, 127, 126, 125, 122, 119, 118, 47, 35, 32.

2.7.6.   *N*-[4-Chlorophenyl-(2-hydroxynaphthalen-1-yl)methyl]-benzamide. White solid, ^{1}H NMR (DMSO-d$_6$) δ = 10.05 (br, s, 1H), 8.05–7.99 (m, 6H), 7.44 (br, s, 1H), 7.27–7.24 (m, 4H), 7.057–7.01 (m, 5H), 6.12 (s, 1H); ^{13}C NMR (DMSO-d$_6$): δ = 165, 153, 139, 134, 132, 131, 130, 128, 127, 126, 123, 122, 119, 116, 49.

2.7.7.   *N*-[1-(2-Hydroxynaphthalen-1-yl)butyl]benzamide. White solid, ^{1}H NMR (DMSO-d$_6$) δ = 10.08 (br, s, 1H), 8.12–8.05 (m, 6H), 7.84–7.78 (m, 5H), 7.31 (br, s, 1H), 6.35 (t, 1H), 2.15 (s, 3H), 1.85–1.79 (m, 1H), 1.39–1.33 (m, 1H), 0.98 (t, 3H); ^{13}C NMR (DMSO-d$_6$) δ = 163, 155, 148, 144, 139, 135, 134, 132, 129, 128, 126, 125, 123, 119, 118, 48, 36, 19, 13.

2.7.8.   *N*-[(2-Hydroxynaphthalen-1-yl)(4-hydroxyphenyl)methyl]-benzamide. Light brown solid, ^{1}H NMR (DMSO-d$_6$) δ = 11.24 (br, 1H), 8.93 (br, 1H), 8.12–8.06 (m, 6H), 7.82–7.77 (m, 4H), 7.22–7.15 (m, 5H), 6.78 (s, 1H); ^{13}C NMR (DMSO-d$_6$) δ = 170, 156, 152, 149, 144, 139, 134, 132, 130, 129, 128, 127, 125, 124, 123, 122, 121, 120, 50.

3.   Results and discussion

3.1.   Characterization of inorganic–organic nanohybrid material HPA/TPI-MCM-41

3.1.1.   X-ray diffraction. Fig. 1 and 2 show the small and wide-angle, respectively, X-ray powder diffraction (XRD) patterns of MCM-41, TPI-MCM-41, and HPA/TPI-MCM-41 samples. As Fig. 1 illustrates, reflections are assigned to (100), (110), (200), and (210) planes in the highly ordered 2D hexagonal arrangement of pores with d_{100} spacing of 4.63 nm for pure MCM-41.[27] For TPI-MCM-41 and HPA/TPI-MCM-41, three intense reflections disappeared and only a sharp reflection associated with (100) was observed. The intensity of this reflection after functionalizing with TPI was obviously lower than that of the original MCM-41, which may be ascribed to a pore-filling effect of TPI. After loading of HPA on TPI-MCM-41, the intensity of XRD reflections on HPA/TPI-MCM-41 was weakened further, in comparison with the unmodified MCM-41
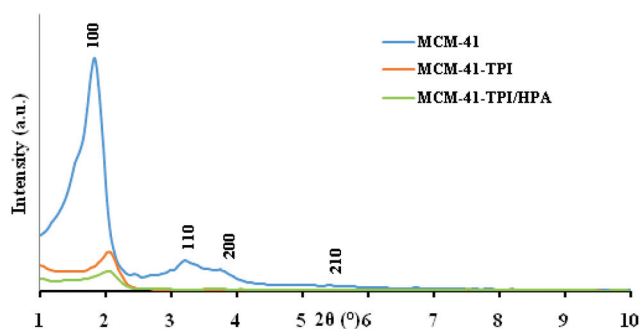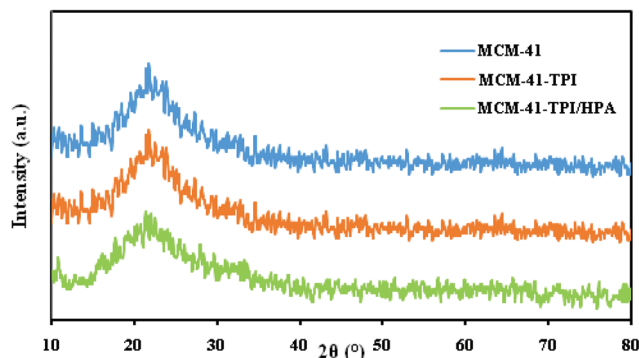

Fig. 2 Wide-angle XRD patterns of MCM-41, TPI-MCM-41 and HPA/TPI-MCM-41.

and pyridine-functionalized MCM-41, due to the incorporation of the heteropolyacid. The broad band between 18° and 30° in the wide-angle XRD patterns of all three compounds (Fig. 2) was characteristic of amorphous silica walls of the pristine material.[28] Notably, no characteristic peak for $H_4SiW_{12}O_{40}$ crystallites (20.5°, 25.4°, 29.4°, 34.6°, and 53.3°) was detected in HPA/TPI-MCM-41.[29] This clearly implied the fine dispersion of the HPA on the support surface.[30]

3.1.2.   SEM and EDX of HPA/TPI-MCM-41. MCM-41 is a short-range amorphous material containing a large number of silanol groups available for grafting. The morphology of the HPA/TPI-MCM-41 nanocatalyst was investigated by SEM as shown in Fig. 3a. This micrograph illustrates that the nanoparticles have a semi-spherical morphology with a narrow size distribution and an average diameter of approximately 80 nm, and $H_4SiW_{12}O_{40}$ is well dispersed on TPI-MCM-41. Concerning the chemical composition of the HPA/TPI-MCM-41 nanocatalyst, energy dispersive X-ray (EDX) analysis was carried out (Fig. 3b). The EDX analysis proved existence of tungsten in addition to silicon in the nanocatalyst indicating silicotungstic acid grafted successfully on MCM-41 mesoporous silica.

3.1.3.   FT-IR spectroscopy. Fig. 4 illustrates FT-IR spectra of MCM-41, TPI-MCM-41, HPA/TPI-MCM-41 and $H_4SiW_{12}O_{40}$. For the parent MCM-41 material, asymmetric and symmetric Si–O–Si characteristic stretching vibrations at 1076 cm^{-1} and 800 cm^{-1} along with Si–OH at 950 cm^{-1} and bending Si–O–Si at 458 cm^{-1} are observed. The broad band around 3450 cm^{-1} is due to the surface silanols and adsorbed water molecules and the band at 1635 cm^{-1} is assigned to the H–O–H bending vibration of the free or absorbed water molecules.[26,31] After modification of MCM-41 with TPI, several new bands appeared. The presence of organic groups was confirmed by observation of the stretching vibrations for C–H aromatic, C–H aliphatic, C=O and C=N at 3070, 2950–2850, 1650 and 1550 cm^{-1} regions, respectively. Decreasing intensities of the O–H and Si–OH stretching vibrations for TPI-MCM-41 indicated substitution of some of the surface silanols groups with TPI reagent. Notably, the stretching vibration band of the NH$_2$ group is completely obscured by the broad stretching vibration band of the O–H group.[32,33] The Keggin structure of

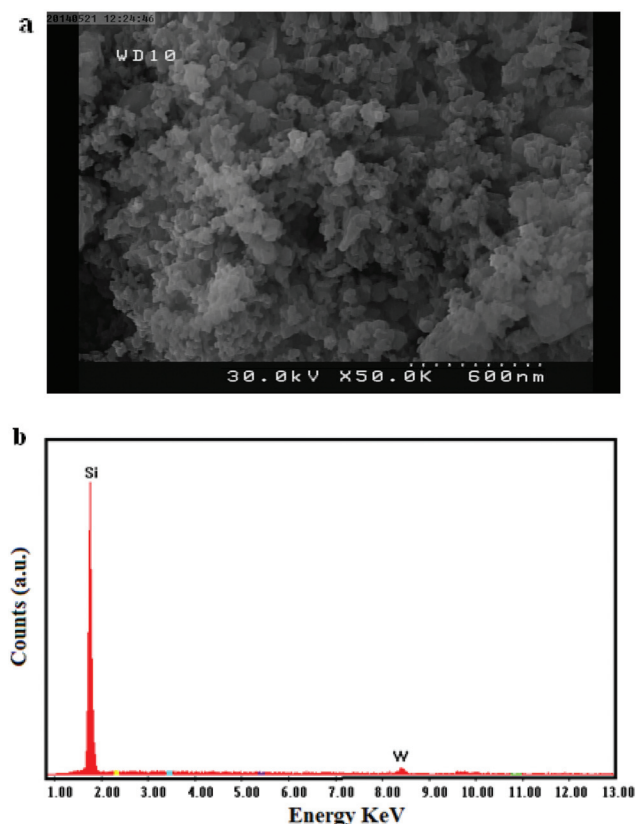**Fig. 1** Sall-angle XRD patterns of MCM-41, TPI-MCM-41 and HPA/TPI-MCM-41.

Fig. 3 SEM micrograph (a) and EDX spectrum (b) of HPA/TPI-MCM-41 nanocatalyst.
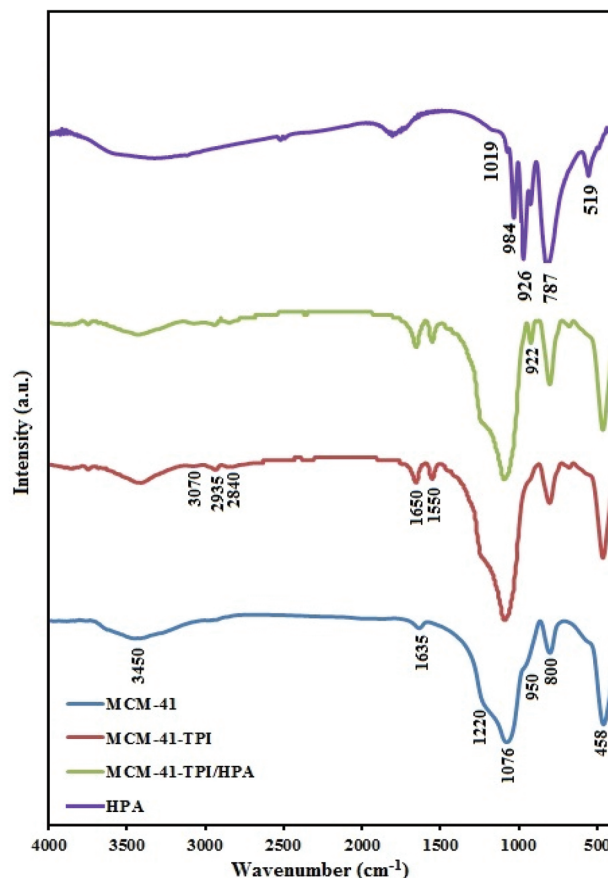
Fig. 4 FT-IR spectra of MCM-41, TPI-MCM-41, HPA/TPI-MCM-41 and $H_4SiW_{12}O_{40}$.

$H_4SiW_{12}O_{40}$ consists of a central SiO_4 tetrahedron surrounded by four W_3O_9 groups formed by edge-sharing octahedrons. These groups are connected to each other by corner-sharing oxygen atoms. The FT-IR spectrum of the parent Keggin $H_4SiW_{12}O_{40} \cdot nH_2O$ showed characteristic stretching and bending vibration bands of H_2O at 3410 and 1620 cm^{-1}, and Si–O and W=O stretching vibrations along with edge-sharing and corner -sharing W–O–W stretching vibrations at 1019, 984, 926 and 787 cm^{-1}, respectively (Fig. 4).[34–39]

Fig. 4 also shows the FT-IR spectrum of the immobilized heteropolyacid on the pyridine-functionalized MCM-41. Although characteristic bands associated with MCM-41-TPI are clearly visible in the spectrum of the prepared nanocatalyst, HPA bands were masked as a result of the strong background of the silica support. Actually, from the characteristic bands in the 700–1100 cm^{-1} region of HPA, only the edge-sharing W–O–W stretching vibration band at 922 cm^{-1} is observed. A slight shift of this band, in comparison with the bulk HPA, is probably due to interaction of the HPA with TPI-MCM-41.[40]

3.1.4. Thermal analysis. TGA-DTA curves of TPI-MCM-41, HPA/TPI-MCM-41 and HPA are illustrated in Fig. 5. TPI-MCM-41 has two weight losses due to the desorption of physisorbed water on the external surface of the crystallites or occluded in MCM-41 mesopores below 150 °C, and the oxidative decomposition of the organic part of TPI between

200–600 °C which is accompanied by exothermic peaks at 380 °C and 512 °C in DTA curves, respectively. According to the weight loss in the TGA curve, the amount of pyridine agent introduced into TPI-MCM-41 was 1.2 mmol g^{-1}.[32,41] On the other hand, thermal analysis of $H_4SiW_{12}O_{40} \cdot nH_2O$ illustrates a major weight loss between 25–300 °C and a minor loss at 350–600 °C. The first weight loss can be related to water loss from $H_4SiW_{12}O_{40} \cdot nH_2O$. These data are corroborated by differential thermal analysis: two main endothermic peaks observed between 25 and 300 °C are attributable to the loss of water molecules. The second minor weight loss probably is associated with the decomposition of the Keggin anion which is accompanied by a sharp and relatively intense exothermic transition in the region of 535 °C.[42–44]

The TGA-DTA curve of the synthesized catalyst is similar to that of the pyridine functionalized material. There are two weight losses below 300 °C due to water loss accompanied with endothermic peaks in the same region and also another weight loss between 300–700 °C which corresponds to the oxidative decomposition of the organic part of TPI and degradation of the heteropolyacid. This is accompanied by exothermic peaks at 386 °C and 512 °C in the DTA curve, respectively. Notably, according to thermal analysis data, the prepared nanohybrid catalyst is stable up to 250 °C.
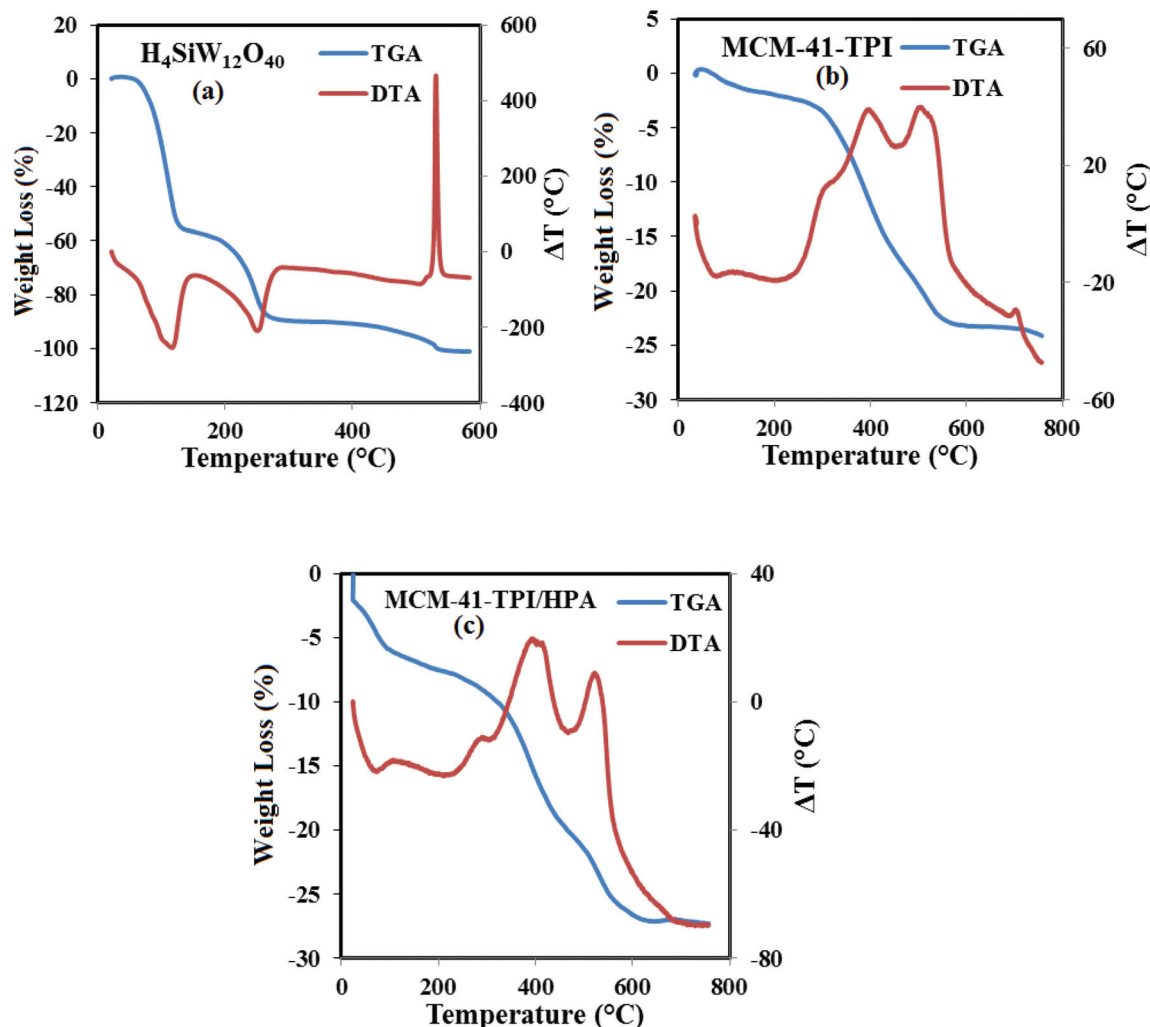
Fig. 5   TGA and DTA analyses for $H_4SiW_{12}O_{40}$ (a), TPI-MCM-41 (b), and HPA/TPI-MCM-41 (c).

3.1.5.   UV-Vis spectroscopy. To determine the extent of HPA loaded on TPI-MCM-41, UV-Vis spectra of solutions containing HPA before and after addition of TPI-MCM-41 were measured (Fig. 6). For this purpose, 1.0 g TPI functionalized MCM-41 mesoporous silica was suspended in 50 ml methanolic solution of silicotungstic acid with an initial concentration of 14 000 ppm. The suspension was refluxed for 4 h, and then the catalyst was removed by filtration and the adsorption spectrum was recorded. Comparison of the absorbance band with calibration curves for standard solutions of HPA in methanol after 240 min refluxing showed that the heteropolyacid concentration had declined to 8600 ppm. This indicated that 5400 ppm HPA grafted to 1.0 g of TPI-MCM-41, which corresponds to 0.0933 mmol g^{-1} of HPA on the support. The band observed in the UV-Vis spectrum at 268 nm is the characteristic band of $H_4SiW_{12}O_{40}$ and corresponds to the O→W charge transfer band.[42–44] For confirmation of HPA loading on the support, 0.01 g of heterogeneous catalyst was suspended in 100 μL HF to remove the siliceous skeleton. Then the mixture was stirred for 4 h and filtered, and the solution was diluted
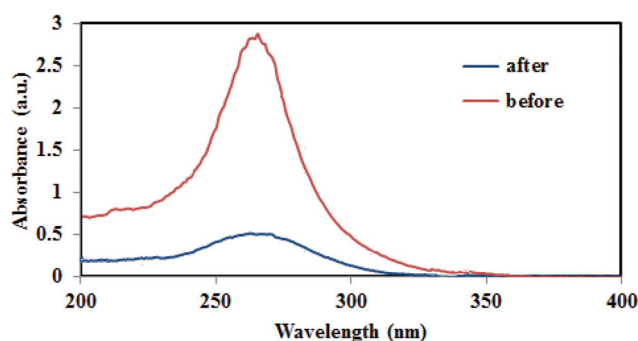
Fig. 6   UV-Vis spectra of $H_4SiW_{10}O_{40}$ before and after immobilization on TPI-MCM-41 after 4 h.

with distilled water to 25 ml. Analysis of the solution by ICP-OES showed the presence of 80 ppm tungsten in the sample, which corresponds to 0.09 mmol g^{-1} HPA on the TPI-MCM-41 support. This finding is in good agreement with the result of UV-Vis analysis. Comparison of TPI loading on
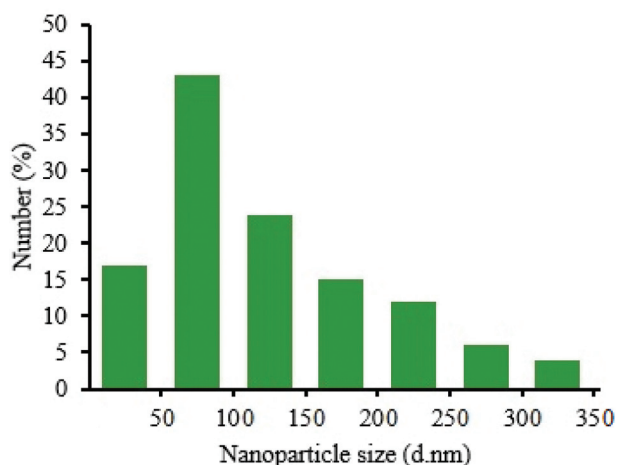
Fig. 7 Size distribution histogram of the synthesized HPA/TPI-MCM-41 from DLS analysis.

Table 1 Effect of the heteropolyacid nature and structure on the efficacy of the catalytic system[a]

Catalyst	Structure	Time (min)	Yield (%)
$H_3PMo_{12}O_{40}$	Keggin	35	78
$H_3PW_{12}O_{40}$	Keggin	25	79
$H_6P_2W_{18}O_{62}$	Wells-Dawson	15	75
$H_6P_2Mo_{18}O_{62}$	Wells-Dawson	20	79
$H_4SiW_{12}O_{40}$	Si-substituted Keggin	7	95
$H_4SiW_9Mo_2O_{40}$	Si-substituted mixed metal lacunary Keggin	15	75
$H_4SiW_9Mo_3O_{40}$	Si-substituted mixed metal Keggin	15	80

[a] Reactions were carried out as described in the experimental section. 0.5 mol% of catalyst was used in each case.

MCM-41 and HPA loading on TPI-MCM-41 showed that about 8% of pyridine groups on the surface of MCM-41 are co-ordinated to the Keggin heteropolyacid.

3.1.6. Dynamic light scattering (DLS) analysis of HPA/TPI-MCM-41. HPA/TPI-MCM-41 was suspended in ethanol and the hydrodynamic particles size was determined by measuring the dynamic light scattering (Fig. 7). The particle size histogram of the nanohybrid catalyst showed that most of the particles ranged in size from 70–120 nm and possessed an average size of ~75 nm.

3.2. Catalytic tests

3.2.1. Effect of the heteropolyacid nature and structure on the efficacy of the catalytic system. The catalytic activity of $H_4SiW_{12}O_{40}$ was compared with some familiar heteropolyacids in the preparation of N-[(2-hydroxy-naphthalen-1-yl)phenyl-methyl]benzamide (Table 1). All used Keggin and Wells–Dawson heteropolyacids are strong acids and behave as good catalysts in the target transformation.[45] Although Wells–Dawson heteropolyacids showed better catalytic activity than Keggin $H_3PW_{12}O_{40}$ and $H_3PMo_{12}O_{40}$, the two Si-substituted mixed metal Keggin heteropolyacids showed comparable activity. Among the examined heteropolyacids, $H_4SiW_{12}O_{40}$ as Si-substituted Keggin-type heteropolyacid showed clearly the best catalytic activity. The different reactivity patterns observed in Table 1 can be explained considering many factors such as total acidity of the heteropolyacid, negative charge density smeared over oxygen atoms, structure, and modality of adsorption of organic reagents to the bulk of the heteropolyacid during reaction.[46,47]

3.2.2. Studying the catalytic activity of some modified mesoporous nanomaterials and heteropolyacids compared to HPA/TPI-MCM-41. There are several reports on the electrostatic anchoring of different heteropolyacids on modified solid supporting materials with a suitable organic linker. This strategy is a beneficial solution to overcome leaching of catalytic

Table 2 Effects of the type of solid support material, organic linker, and heteropolyacid on the efficacy of the catalytic reaction[a]

Entry	Catalyst	Mol% (based on HPA)	Time (min)	Yield (%)	Ref.
1	$H_6P_2W_{18}O_{62}$/TPI-(Al)SBA-15	0.16	20	51	46
2	$H_5PW_{10}V_2O_{40}$/TPI-SBA-15	0.10	30	45	48
3	$H_5PW_{10}V_2O_{40}$/Pip-SBA-15	0.10	30	33	49
4	$H_6P_2W_{18}O_{62}$/TPI-CNT	—	25	55	—
5	$H_4SiW_{12}O_{40}$/TPI-MCM-41	0.13	20	94	This work

[a] Reaction conditions selected as in the experimental section. Reactions were performed with 15 mg of each catalyst. CNT refers to carbon nanotubes. TPI and Pip refer to N-[3-(triethoxysilyl)propyl] isonicotinamide and 1-[3-(triethoxysilyl)propyl]piperazine, respectively.

active sites from the supporting material. Therefore, we were interested to study the effect of the type and nature of some mesoporous supports modified with the two organic linkers TPI and 1-[3-(triethoxysilyl)propyl]piperazine (Pip) which were electrostatically anchored to $H_5PW_{10}V_2O_{40}$ and $H_6P_2W_{18}O_{62}$ heteropolyacids (Table 2). The results revealed that TPI behaved better than the other linker in the case of SBA-15. Moreover, among different supports such as MCM-41, SBA-15, (Al)SBA-15, and CNT, the first was the best. Therefore, mesoporous silica MCM-41, containing silanol functional groups with high specific surface area which opened a wide field of applications in chemical industries, was selected as the best solid support in this study.

3.2.3. Studying the catalytic activity of the ingredients composing HPA/TPI-MCM-41. Fig. 8 compares the catalytic activity of HPA/TPI-MCM-41 with $H_4SiW_{12}O_{40}$, TPI-MCM-41, and MCM-41 in the preparation of α-amidoalkyl-β-naphthol under the standard reaction conditions. 4 mg of $H_4SiW_{12}O_{40}$ provided 68% yield of the desired product after 20 min; whereas, 15 mg of the inorganic–organic hybrid material HPA/TPI-MCM-41, which includes the same amount of HPA (4 mg), achieved 94% yield after a short time of 20 min. The unmodified MCM-41 and the modified material TPI-MCM-41 were also catalytically active; these materials led to 11% and 24% of
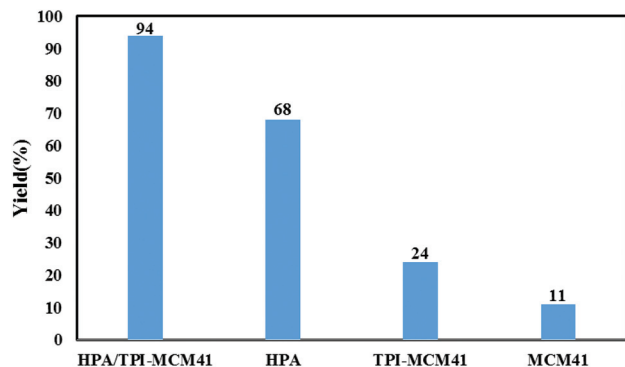
Fig. 8 Studying the catalytic activity of HPA/TPI-MCM-41 ingredients. 4 mg HPA and 15 mg of other components were used. Data were obtained after 20 min.

Fig. 10 Effect of reaction temperature on the condensation reaction catalyzed by HPA/TPI-MCM-41.

product, respectively, after the same time. Although the components of the hybrid material showed slight catalytic activity, HPA/TPI-MCM-41 performed the best in the desired organic transformation. Obviously, immobilizing the heteropolyacid onto the modified solid material TPI-MCM-41 increased its catalytic activity towards the condensation reaction.

3.2.4. Effect of catalyst concentration. The catalytic efficiency of the heterogeneous HPA/TPI-MCM-41 was investigated for the preparation of α-amidoalkyl-β-naphthol with various amounts of catalyst (Fig. 9). It was found that only 15% yield was attained after the long time of 3 h. In order to evaluate the appropriate catalyst amount, a model reaction was carried out by applying 5–40 mg HPA/TPI-MCM-41. It was found that 5 mg of catalyst afforded 45% yield after 1 h. This finding revealed that the heterogeneous catalyst exhibited high catalytic activity in the desired transformation. As expected, the percentage yield was increased with enhancing catalyst concentration. However, higher amounts of catalyst (>15 mg) neither increased nor lowered the percentage yield. Therefore, 15 mg of catalyst was chosen as the optimal quantity to push the reaction forward.

3.2.5. Effect of temperature on the condensation reaction. Effect of reaction temperature on the preparation of α-amidoalkyl-β-naphthol was investigated in the presence of HPA/TPI-MCM-41 nanoparticles (15 mg) under solvent-free conditions (Fig. 10). Yield of the desired product was enhanced by increasing the temperature from 25 to 130 °C. It was observed that the reaction did not sufficiently proceed at room temperature and only 26% yield was achieved after 180 min; whereas, at 60 °C the reaction poorly proceeded and maximum conversion (52%) was attained after 75 min. The best result was achieved at 100 °C. Further increase in temperature did not significantly improve the conversion. Therefore, we kept the reaction temperature at 100 °C.

3.2.6. Synthesis of different α-amidoalkyl-β-naphthols in the presence of HPA/TPI-MCM-41 under solvent-free conditions. The generality of the present protocol was evaluated by examining structurally diverse aromatic and aliphatic aldehydes carrying either electron-withdrawing, electron-donating, or halogen groups on the aromatic rings (Table 3). The reaction of aldehydes bearing electron-withdrawing groups such as 4-nitrobenzaldehyde (entry 2) was successful and gave the corresponding product in 70% yield after 35 min; but lower yields were achieved and longer reaction times were necessary for aldehydes involving strong electron-donating groups such as 4-(N,N′-dimethylamino)benzaldehyde (entry 14). In addition to the electronic factors, steric congestion also affected the reaction in terms of time and yield. Comparison of entries 7 and 8 indicates that existence of bulky substituents on the ortho-positions of the phenyl ring decreased the yield and needed longer reaction time.

3.3. Comparison of the catalytic activity of HPA/TPI-MCM-41 nanoparticles with some reported catalysts

The activity of the present heterogeneous catalyst $H_4SiW_{12}O_{40}$/TPI-MCM-41 was studied compared to some reported catalysts (Table 4). The reaction of β-naphthol with benzaldehyde and

Fig. 9 Effect of catalyst concentration on the desired condensation reaction.

Table 3 Synthesis of different α-amidoalkyl-β-naphthol derivatives in the presence of HPA/TPI-MCM-41 under solvent-free conditions[a]

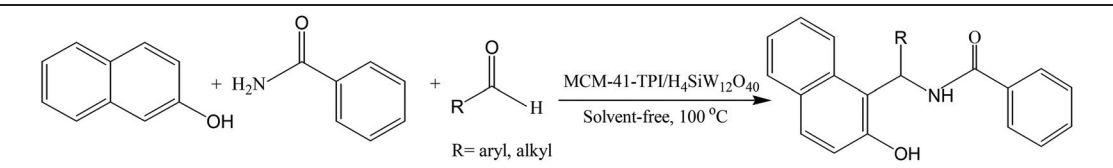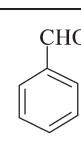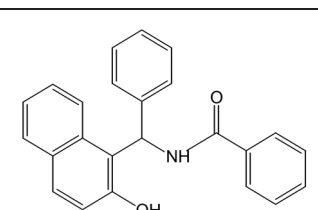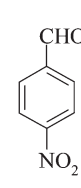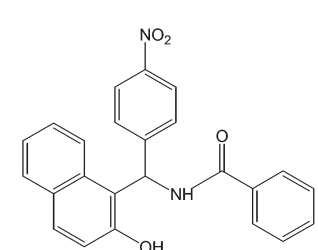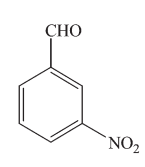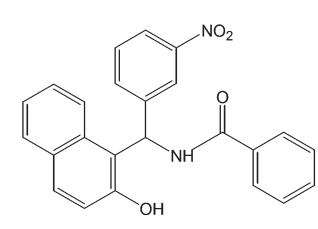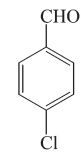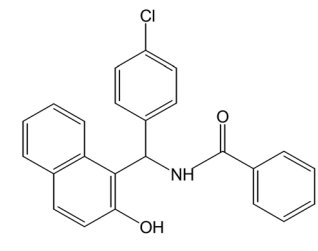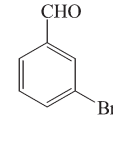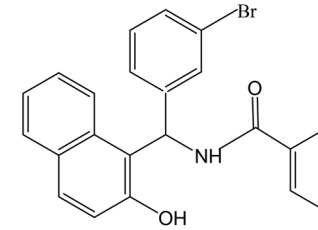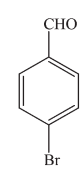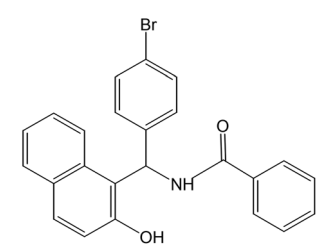| Entry	Aldehyde	Time (min)	Yield (%)	m.p./lit. m.p. (°C)	Product
1	CHO	20	94	235–236/235–237[50]	
2	CHO, NO$_2$	35	70	237–238/238–240[51]	
3	CHO, NO$_2$	45	85	232–234/232–234[52]	
4	CHO, Cl	45	83	175–176/176–177[53]	
5	CHO, Br	35	83	230–232	
6	CHO, Br	35	45	183–185/182–184[54]	

Table 3 *(Contd.)*
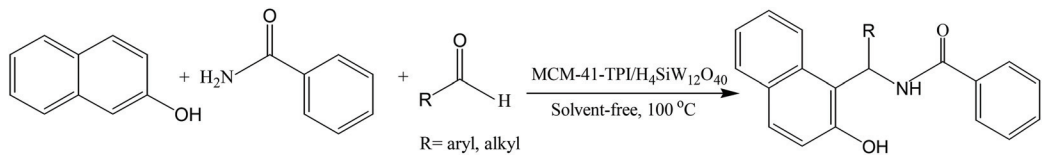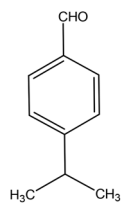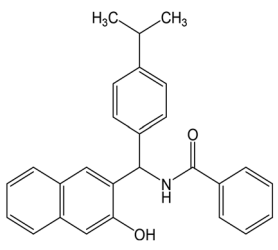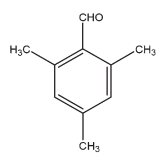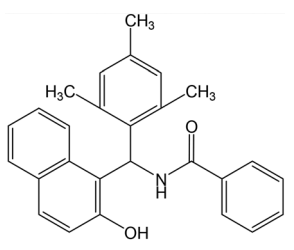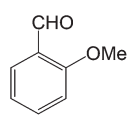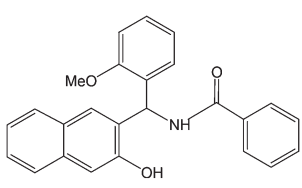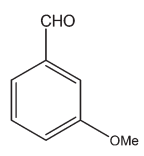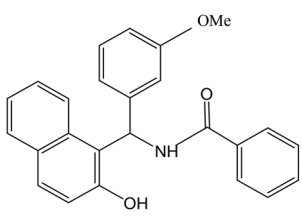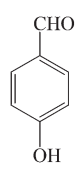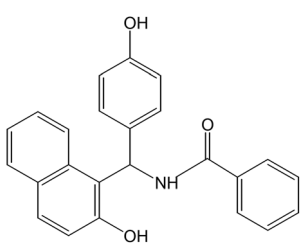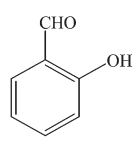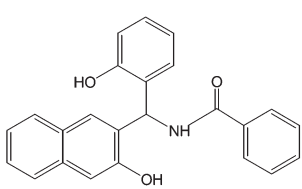
Entry	Aldehyde	Time (min)	Yield (%)	m.p./lit. m.p. (°C)	Product
7		40	65	208/210[22]	
8		60	18	245–246	
9		25	55	266–267/266–267[55]	
10		35	55	169–171/168–170[54]	
11		30	87	220–223	
12		55	48	234–236	

Table 3 *(Contd.)*

Entry	Aldehyde	Time (min)	Yield (%)	m.p./lit. m.p. (°C)	Product
13		30	89	236/234[54]	
14		45	50	221–222/220–221[55]	
15		45	48	247–248	
16		60	57	233–234/233–235[53]	

[a] Reactions were carried out as described in the experimental section. Yields refer to the isolated pure products. The desired products were characterized by comparison of their physical data with those of known compounds.

Table 4 Comparison of the catalytic efficiency of HPA/TPI-MCM-41 nanocatalyst with some reported catalysts for the reaction of β-naphthol with benzaldehyde and benzamide

Entry	Catalyst	Catalyst (mol% or g); conditions	Time (h)	Yield (%)	Ref.
1	HPA/TPI-MCM-41	15 mg; solvent-free, 100 °C	0.4	94	This work
2	Montmorillonite K10	0.1 g; solvent-free, 125 °C, neat	1.5	78	54
3	$H_3PMo_{12}O_{40}$	1.6 mol%; CH_3COOEt, 65 °C	4	92	56
4	NKC-9	0.17 g; $CHCl_3$, 65 °C	4	89	57
5	$H_3PMo_{12}O_{40}/SiO_2$	3.17 mol%; solvent-free, 120 °C	1	82	58
6	Sulfamic acid	2.5 mol%; solvent-free, 28–30 °C	4	74	59
7	1-Hexanesulphonic acid sodium salt	10 mol%; MW irradiation	0.1	92	60

benzamide for the synthesis of the corresponding α-amidoalkyl-β-naphthol was selected as a model reaction and the comparison was in terms of mol% of the catalyst, temperature, reaction time, and percentage yields. Obviously, the present new nanohybrid material is better than most of the mentioned catalysts. Although some introduced additives catalyzed the reaction, even though at lower temperature, they required toxic and/or expensive solvents, higher mol% of catalyst, and longer reaction times.

3.4. Reusability and reproducibility of HPA/TPI-MCM-41 nanocatalyst

A major drawback of homogeneous free HPA is the separation and recovery of the catalyst when the reaction is completed. Heterogenization of HPA *via* anchoring to TPI-MCM-41 is an attractive strategy allowing easy separation. Moreover, reusability and regeneration of the catalyst reduce wastage and production of wasteful materials. To investigate the reusability of HPA/TPI-MCM-41, it was easily separated from the reaction mixture and washed thoroughly with ethanol. Then, the catalyst was slowly dried in air and then was activated in a vacuum oven at 80 °C for 2 h. Finally, the recycled catalyst was reused for another condensation reaction. Findings revealed nearly the same catalytic activity as for the fresh catalyst, albeit with slightly decreasing activity (Fig. 11 and 12). Moreover, to ensure reproducibility of the transformation, repeated typical experiments were carried out under identical reaction conditions. The obtained yields were found to be reproducible within ±3% variation. It could thus be concluded that HPA/TPI-MCM-41 could be a satisfactory catalyst for this reaction with high activity and good reusability.

3.5. Hot filtration test

To establish that the catalytic activity was generated from the heterogeneous nanohybrid catalyst, and not from the leached heteropolyacid in the reaction mixture, a hot filtration test was planned. In this technique, the condensation reaction of β-naphthol (1.0 mmol), aldehyde (1 mmol), and benzamide (1.2 mmol) in a small test tube equipped with a condenser performed at 100 °C for 25 min in the presence of HPA/
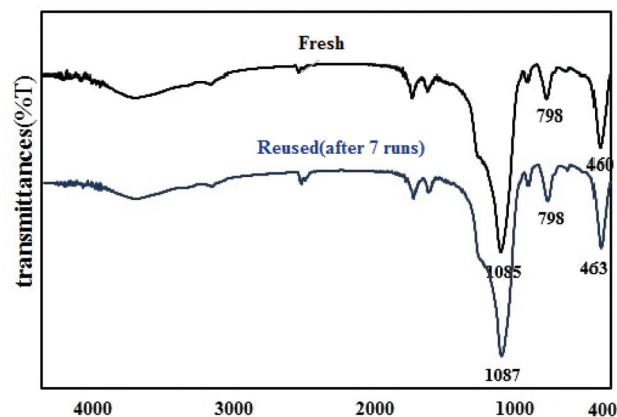

Fig. 12 FT-IR spectra of fresh and recovered catalysts.

TPI-MCM-41 (15 mg). At this stage, the yield of the product was 76%. Then, the solid catalyst was filtered off under hot conditions and with the filtrate, which was obtained after separation of the catalyst, the reaction was continued for another 25 min at the same reaction temperature. However, no corresponding increase in yield beyond 76% was observed. This result clearly confirmed the heterogeneous nature of the mesoporous nanohybrid catalyst in this condensation reaction and no leaching of the heteropolyacid occurred during the course of the reaction.

3.6. Proposed reaction pathway for the catalytic system

Scheme 3 shows a plausible reaction pathway for the three-component condensation reaction.[61,62] Presumably, the reaction proceeded *via ortho*-quinonemethide (I) formed by the nucleophilic addition of β-naphthol to the carbonyl group of the aldehyde which was activated by the nanocatalyst. Finally, (I) reacts with the amide *via Michael* addition to afford the desired 1-amidoalkyl-2-naphthol. According to this mechanism, electron-releasing substituents deactivate the aldehyde to accept the nucleophilic attack of β-naphthol; however, electron-withdrawing groups activate the carbonyl group of the aldehyde.
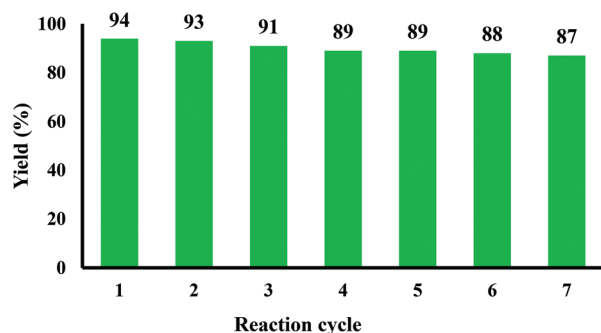
4. Conclusions

HPA/TPI-MCM-41 catalyst was prepared from commercially available starting materials, and efficiently catalyzed the synthesis of 1-amidoalkyl-2-naphthols through the condensation of β-naphthol and benzaldehyde with benzamide under solvent-free, one-pot, and multi-component conditions. The advantages of this method include short reaction time, high yields, and easy purification as well as the reusability and economic viability of the catalyst. This protocol is developed as a safe and convenient alternate method by applying an eco-friendly and highly reusable catalyst.

Fig. 11 Reusability of HPA/TPI-MCM-41 nanocatalyst.
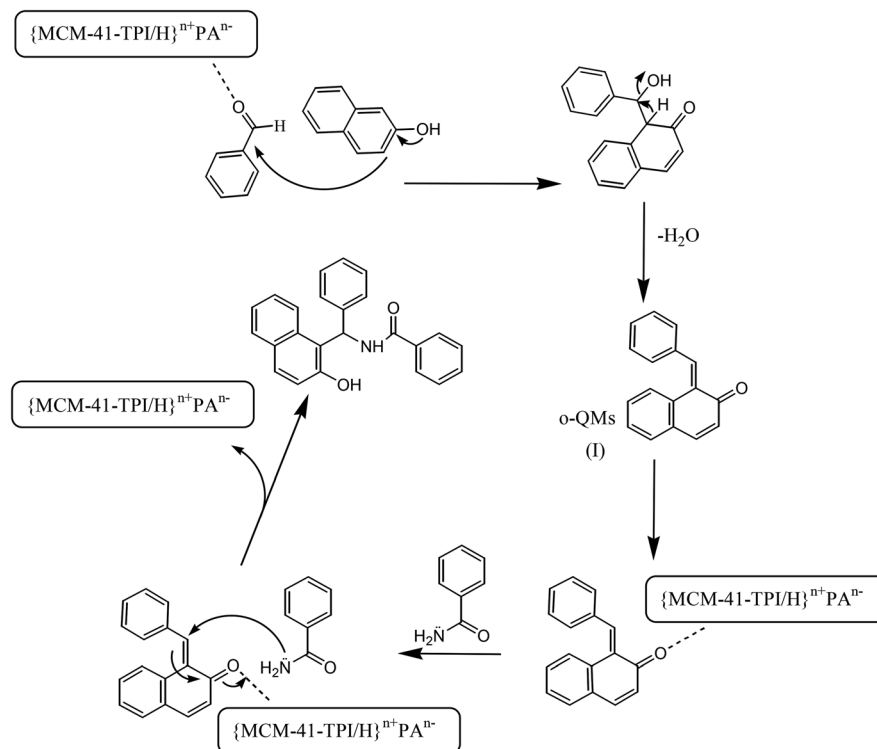
Scheme 3 Proposed reaction pathway for the preparation of 1-amidoalkyl-2-naphthol catalyzed by HPA/TPI-MCM-41.

Acknowledgements

Notes and references

1 A. P. Wight and E. Davis, *Chem. Rev.*, 2002, **102**, 3589.
2 C. Sanchez and F. Ribot, *New J. Chem.*, 1994, **18**, 1007.
3 S. Udayakumar, S. Ajaikumar and A. Pandurangan, *Appl. Catal., A*, 2006, **302**, 86.
4 B. E. Ali, J. Tijani, M. Fettouhi, M. E. Faer and A. A. Arfaj, *Appl. Catal., A*, 2005, **283**, 185.
5 R. R. Jermy and A. Pandurangan, *Appl. Catal., A*, 2005, **295**, 185.
6 R. Maheswari, K. Shanthi, T. Sivakumar and S. Narayanan, *Appl. Catal., A*, 2003, **248**, 291.
7 R. Tayebee and B. Maleki, *J. Chem. Sci.*, 2013, **125**, 335.
8 M. Vallet-Regi, A. Ramila, R. P. Del Real and J. Perez-Pariente, *Chem. Mater.*, 2001, **13**, 308.
9 Y. F. Zhu, J. L. Shi, W. H. Shen, X. P. Dong, J. W. Feng, M. L. Ruan and Y. S. Li, *Angew. Chem., Int. Ed.*, 2005, **44**, 5083.
10 S. P. Rigby, M. Fairhead and C. F. van der Walle, *Curr. Pharm. Des.*, 2008, **14**, 1821.
11 X. S. Zhao, G. Q. Lu, A. J. Whittaker, G. J. Millar and H. Y. Zhu, *J. Phys. Chem. B*, 1997, **101**, 6525.
12 S. Inagaki, S. Guan, Y. Fukushima, T. Ohsuna and O. Terasaki, *J. Am. Chem. Soc.*, 1999, **121**, 9611.
13 T. Dingermann, D. Steinhilber and G. Folkers, *Mol. Biol. Med. Chem.*, 2004, **21**, 381.
14 S. Knapp, *Chem. Rev.*, 1995, **95**, 1859.
15 Y. Kusakabe, J. Nagatsu, M. Shibuya, O. Kawaguchi, C. Hirose and S. Shirato, *J. Antibiot.*, 1972, **2**, 44.
16 S. Remillard, L. I. Rebhun, G. A. Howie and S. M. Kupchan, *Science*, 1975, **189**, 1002.
17 J. L. Peglion, J. Vian, B. Gourment, N. Despaux, V. Audinot and M. Millan, *Bioorg. Med. Chem. Lett.*, 1997, **7**, 881.
18 R. D. Clark, J. M. Caroon, A. F. Kluge, D. B. Repke, A. P. Roszkowski, A. M. Strosberg, S. Baker, S. M. Bitter and M. D. Okada, *J. Med. Chem.*, 1983, **26**, 657.
19 S. Samantaray, G. Hota and B. G. Mishra, *Catal. Commun.*, 2011, **12**, 1255.
20 D. Kundu, A. Majee and A. Hajra, *Catal. Commun.*, 2010, **11**, 1157.
21 M. A. Amrollahi, F. Mirjalili and H. Emtiazi, *J. Chem. Sci.*, 2013, **125**, 561.
22 M. Zandi and A. R. Sardarian, *C. R. Chim.*, 2012, **15**, 365.
23 E. North, *Inorg. Synth.*, 1939, **1**, 129.
24 C. Nunes, A. Valente, M. Pillinger, A. Fernandes, C. Romão, J. Rocha and I. Gonçalves, *J. Mater. Chem.*, 2002, **12**, 1735.

25 J. Hoogbomm, P. M. L. Garcia and M. B. Otten, *J. Am. Chem. Soc.*, 2005, **127**, 11047.

26 T. P. B. Nguyen, J.-W. Lee, W. G. Shim and H. Moon, *Microporous Mesoporous Mater.*, 2008, **110**, 560.

27 Z. Qu, D. Chen, Y. Sun and Y. Wang, *Appl. Catal., A*, 2014, **487**, 100.

28 H. Zhao, J. C. Zhou, H. Luo, C. Y. Zeng, D. H. Li and Y. J. Liu, *Catal. Lett.*, 2006, **108**, 49.

29 L. Pesaresi, D. R. Brown, A. F. Lee, J. M. Montero, H. Williams and K. Wilson, *Appl. Catal., A*, 2009, **360**, 50.

30 Z. Shanhui, Z. Yulei and H. Shunli, *Catal. Lett.*, 2012, **142**, 267.

31 E. Vunain, N. Opembe, K. Jalama, A. Mishra and R. Meijboom, *J. Therm. Anal. Calorim.*, 2014, **115**, 1487.

32 M. Behbahani, A. Ali Akbari, M. M. Amini and A. Bagheri, *Anal. Methods*, 2014, **6**, 8785.

33 Y. Shuijin, Y. Xieqing and S. Shaomin, *Front. Chem. China*, 2006, **1**, 82.

34 M. Ammam and J. Fransaer, *J. Electrochem. Soc.*, 2011, **158**, A14.

35 F. J. Berry, G. R. Derrick and M. Mortimer, *Polyhedron*, 2014, **68**, 17.

36 G. Yang, Y. Pan, F. Gao, J. Gong, X. Cui, C. Shao, Y. Guo and L. Qu, *Mater. Lett.*, 2005, **59**, 450.

37 L. B. Yang, Y. H. Shen, A. J. Xie, J. J. Liang and B. C. Zhang, *Mater. Res. Bull.*, 2008, **43**, 572.

38 Q. Li, Z. Jin, Z. Peng, Y. Li, S. Li and G. Lu, *J. Phys. Chem. C*, 2007, **111**, 8237.

39 Q. Zhang, Y. Tan, C. Yang and Y. Han, *J. Mol. Catal. A: Chem.*, 2007, **263**, 149.

40 W. Chu, X. Yang, Y. Shan, X. Ye and Y. Wu, *Catal. Lett.*, 1996, **42**, 201.

41 R. Tayebee, M. M. Amini, H. Rostamian and A. Aliakbari, *Dalton Trans.*, 2014, **43**, 1550.

42 Y. Q. Zhang, L. H. Gao, K. Z. Wang, H. J. Gao and Y. L. Wang, *J. Nanosci. Nanotechnol.*, 2008, **8**, 1248.

43 K. Z. Wang and L. H. Gao, *Mater. Res. Bull.*, 2002, **37**, 2447.

44 J. Gong, X. J. Cui, Z. W. Xie, S. G. Wang and L. Y. Qu, *Synth. Met.*, 2002, **129**, 187.

45 R. Tayebee, F. Nehzat, E. Rezaei-Seresht, F. Z. Mohammadi and E. Rafiee, *J. Mol. Catal. A: Chem.*, 2011, **351**, 154.

46 R. Tayebee, M. M. Amini, S. Pouyamanesh and A. Aliakbari, *Dalton Trans.*, 2015, **44**, 5888.

47 R. A. Marcus, *Annu. Rev. Phys. Chem.*, 1964, **15**, 155.

48 R. Tayebee, M. M. Amini, F. Nehzat, O. Sadeghi and M. Armaghan, *J. Mol. Catal. A: Chem.*, 2013, **366**, 140.

49 R. Tayebee, M. M. Amini, M. Ghadamgahi and M. Armaghan, *J. Mol. Catal. A: Chem.*, 2013, **366**, 266.

50 R. R. Nagawade and D. B. Shinde, *Acta Chim. Slov.*, 2007, **54**, 642.

51 S. A. M. K. Ansari, N. S. Jiaprakash, D. K. S. Nagnnath, W. Pravin and D. B. Shinde, *Indian J. Chem. Technol.*, 2010, **17**, 71.

52 M. Wang, Y. Liang, T. T. Zhang and J. J. Gao, *Chin. Chem. Lett.*, 2012, **23**, 65.

53 G. H. Mahdavinia and M. A. Bigdeli, *Chin. Chem. Lett.*, 2009, **20**, 383.

54 S. Kantevari, S. V. N. Vuppalapati and L. Nagarapu, *Catal. Commun.*, 2007, **8**, 1857.

55 G. C. Nandi, S. Samai, R. Kumar and M. S. Singh, *Tetrahedron Lett.*, 2009, **50**, 7220.

56 J. Wen-Qing, A. Li-Taoa and Z. Jian-Ping, *Chin. Chem. Lett.*, 2008, **26**, 1697.

57 A. Li-Tao, L. Xiao-Huab, D. Fei-Qingb, J. Wen-Qingb and Z. Jian-Ping, *Chin. J. Chem.*, 2008, **26**, 2117.

58 A. Zare, A. R. Hasaninejad, E. Rostami, A. R. Moosavi-zare, N. Pishahang, M. Roshankar, F. Khedri and M. Khedri, *Electron. J. Chem.*, 2010, **7**(4), 1162.

59 S. B. Patil, P. R. Singh, M. P. Surpur and S. D. Samant, *Ultrason. Sonochem.*, 2007, **14**, 515.

60 K. S. Niralwad, B. B. Shingate and M. S. Shingare, *Chin. Chem. Lett.*, 2011, **22**, 551.

61 M. M. Khodaei, A. R. Khosropour and H. Moghanian, *Synlett*, 2006, 916.

62 S. B. Patil, P. R. Singh, M. P. Surpur and S. D. Samant, *Synth. Commun.*, 2007, **37**, 1659.